Marine Geology 418 (2019) 106040

Contents lists available at ScienceDirect

Marine Geology

journal homepage: www.elsevier.com/locate/margo

# Observations of wave influence on alongshore ebb-tidal delta morphodynamics at Oregon Inlet, NC

Joshua Humberston[a,b,*], Thomas Lippmann[a], Jesse McNinch[b]

[a] Dept. of Earth Sciences, University of New Hampshire Center for Coastal and Ocean Mapping, Joint Hydrographic Center Chase Ocean Engineering Lab, 24 Colovos Road, Durham, NH 03824, United States of America

[b] Coastal and Hydraulics Laboratory, Coastal Observations and Analysis Branch, U.S. Army Engineer Research and Development Center Field Research Facility, 1261 Duck Rd. Kitty Hawk, NC 27949, United States of America

ARTICLE INFO

Editor: Edward Anthony

ABSTRACT

A Radar Inlet Observation System (RIOS) collected hourly X-band radar data at the wave dominated Oregon Inlet, NC, for 9 months from September 2016 to May 2017. The intensity of the radar backscatter, predominantly associated with surface wave shoaling and breaking, was time-averaged to provide an implied measure of bedforms superimposed on the ebb-tidal delta. Eulerian and Lagrangian motion tracking analyses determined the bedform alongshore migration rates over the study period; these were found to be significantly correlated to estimates of longshore sediment flux based on offshore wave parameters given by Ashton and Murray (2006). Although the exact magnitude of sediment transport cannot be directly estimated from bedform migration, the correlation does support an underlying assumption that sediment transport varies proportionally in both magnitude and direction to average bedform movements. The implications of these findings were further explored through application of the sediment transport model to a year long period of continuous offshore wave data (20 Oct 2016 to 20 Oct 2017). The predicted net transport of 90,000 $m^3$ southward during this year is consistent with a previous estimate of inlet bypassing (Dolan and Glassen 1973). However, pronounced and opposing seasonal transport patterns were an order of magnitude higher than the yearly net, and could lead to significant interannual variability in alongshore sediment transport with similar dynamic response in ebb-delta morphodynamics at Oregon Inlet.

## 1. Introduction

Tidal inlets and their associated delta systems are dynamic sedimentary coastal features that can change substantially on long (monthly to yearly) and short (individual storm) time scales and have the potential to significantly alter local sediment transport patterns (e.g., O'Brien and Zeevaert, 1969; Hayes et al., 1970; Bruun, 1978; Hayes, 1980; FitzGerald, 1988; FitzGerald, 1996; Elias et al., 2003; Fiechter et al., 2006; Pacheco et al., 2008). However, understanding and predicting inlet sediment dynamics has proven difficult, largely owing to the complex interactions of waves and currents with the seabed that contribute to variations in formation and maintenance of channels and shoals (e.g. Aubrey and Giese, 1993; FitzGerald, 1996; Elias et al., 2003; Davidson-Arnott, 2010; Olabarrieta et al., 2011; Chen et al., 2014). Complicating the problem is that flood- and ebb-tidal deltas are generally superimposed with complex and highly variable bedforms ranging in scale from several to tens of meters (Hayes, 1980; Komar, 1996; FitzGerald et al., 2000; Pianca et al., 2014).

General tidal delta properties are categorized reasonably well from knowledge of local tidal magnitude, wave climate, and gross bathymetry (Hayes, 1980; Boothroyd, 1985). The mechanisms of delta evolution and sediment bypassing are less clear. At wave dominated inlet systems, classic theory suggests sediment bypasses the inlet via bedforms (referred to as swash bars) that migrate along a continuous pathway over the ebb-delta's terminal lobe (FitzGerald, 1982). The underlying assumption is that sediment transport is in the direction of bedform migration. The details of this process are not well constrained, at least in part because of limited observational data of bedform morphodynamics and sediment transport over the scales of complexity existing at tidal inlet systems (Komar, 1996; Herrling and Winter, 2018).

In this work, we examine patterns of implied bedform movements

* Corresponding author at: Dept. of Earth Sciences, University of New Hampshire Center for Coastal and Ocean Mapping, Joint Hydrographic Center Chase Ocean Engineering Lab, 24 Colovos Road, Durham, NH 03824, United States of America.

*E-mail addresses:* jhumberston@ccom.unh.edu (J. Humberston), lippmann@ccom.unh.edu (T. Lippmann), Jesse.McNinch@usace.army.mil (J. McNinch).

https://doi.org/10.1016/j.margeo.2019.106040
Received 16 October 2018; Received in revised form 26 July 2019; Accepted 26 August 2019
Available online 29 August 2019

observed from remotely sensed time-averaged breaking patterns on the ebb tidal delta of the wave dominated Oregon Inlet. These patterns, quantified by a spatially averaged migration rate, are compared to the alongshore sediment transport model of Ashton and Murray (2006). The study provides new observational evidence that alongshore bedform migration at the inlet is consistent with wave forcing that drives a net southerly sediment transport that bypasses the inlet, although with substantial seasonal variability. It should be noted that, while bedform morphology is generated by gradients in sediment transport, comparisons of bedform movements with sediment transport formulae are based on an implied assumption herein that sediment transport is in the direction of the bedform migration, an assumption made in many previous inlet and delta studies (e.g., Robinson, 1975; O'Connor et al., 2011; Pianca et al., 2014; Ridderinkohf et al., 2016; and others).

### 1.1. Remote sensing of bedforms

Breaking waves and rapidly changing shallow bathymetry at tidal inlets render most sonar surveys difficult, expensive, and their results of temporally limited relevance. Consequently, several alternative survey procedures have been developed to circumvent these issues, including remote sensing techniques based on optical, lidar, and radar measurement devices that have proven effective at acquiring evolutionary information in energetic inlet environments (Holman and Haller, 2013; Montreuil et al., 2014). Lidar (Light Detection and Ranging) observations from airborne platforms are valuable owing to their very high spatial resolution and rapid observational methods (Lillycrop et al., 1996; Stockdon et al., 2002; Sallenger et al., 2003); however, costs may be prohibitive and turbid water can often prevent detection of bottom returns. This makes it difficult to acquire long time series of inlet bathymetry and bedform locations at regular time intervals and on time scales of interest (Gao, 2009).

Conversely, video (optical) and X-band radars capitalize on energetic sea states by measuring the surface disturbances associated with surface wave propagation independent of water clarity (Holman and Haller, 2013; Hessner et al., 2014; Pianca et al., 2014; Bergsma et al., 2016). As surface waves transition from deep to shallow water, they begin to shoal; celerity and wavelength are reduced while wave steepness increases. Eventually, wave steepness exceeds a critical threshold and wave breaking occurs (Munk, 1949; Thornton and Guza, 1983).

Continuous recording with high-resolution video captures the optical surface reflection of wave shoaling and breaking processes. In post processing, time series of pixel intensity can be used to estimate wavenumbers and frequencies of the surface waves, and subsequently used to infer bathymetry using the dispersion relation (e.g., Williams, 1947) as demonstrated in commonly employed algorithms such as C-bathy (Holman et al., 2013; Radermacher et al., 2014; Bergsma et al., 2016).

In the nearshore, time-averaged optical observations of wave breaking appear as higher intensity signals. Historically, this has been used as a direct proxy for the morphology of the underlying bathymetry (Lippmann and Holman, 1989; and many others). Sequential time-averaged images can then be used to estimate the evolution of the morphology provided a continuous detectable surface signature is captured (Lippmann and Holman, 1990). A major limitation of optical techniques is that images can only be collected during daytime hours, and the range over which image resolution is reasonable is dependent on the height of the camera system (Holman et al., 1993).

X-band radars use a signal from a different band of the electromagnetic spectrum but can often be used in a similar manner to video observations (Haller and Lyzenga, 2003). The backscatter of a microwave X-band signal from long waves like those on the ocean surface is well modeled by the Composite-Surface Model (CSM) that acts on the Bragg scatterers (Bass et al., 1968; Wright, 1968; Catalán et al., 2014). The backscatter also increases as waves shoal and the angle of incidence is reduced (Lee et al., 1995). As waves break, they produce a highly roughened and near-oblique target, further increasing backscatter (Catalán et al., 2014). The resulting interaction between the X-band signal and the surface has been demonstrably useful for making oceanographic measurements in the nearshore region (Barrick, 1972; Donelan and Pierson Jr, 1987; Trizna, 1997). Compared to visual band observations, X-band radars tend to lack the spatial resolution necessary to resolve multiple frequency peaks in the wave field which, according to the CSM, is due to long wave modulations limiting the observed signal of shorter waves. Still, multiple studies have successfully demonstrated inversion techniques (Bell, 1999; Bell, 2002; McNinch, 2007; Catálan and Haller, 2008).

Radar methods have the attractive attributes that they can be used during day and night time periods, and that radar antennae deployments do not require high elevation platforms. Rotating radars can acquire backscatter measurements over circular regions with diameter in excess of 5 km and with 5 m or better resolution. Because radar systems can be used to sample large surface areas in nearly all-weather conditions, they have become increasingly effective research tools in coastal environments, particularly for examining large-scale coastal behavior.

Yet while many studies have utilized both optical and X-band signals to estimate bottom morphology and bathymetry, there remain complicating factors in using water surface characteristics to estimate bottom morphology. The relation between water depths and wave phase speeds measured by radar and optical techniques can be altered by currents that modify wave numbers. The interactions of currents with surface gravity waves may also increase the surface roughness which has implications for the measured backscatter of an X-band signal (Lyzenga, 1991, 1998; Plant et al., 2010). Haller et al. (2014) have been able to capitalize on this effect by using the increased roughness to image the lateral surface structure of rip currents in the nearshore. For application to estimating the position of bottom features, wave breaking has been shown to be more influenced by bathymetry than by wave-current interactions, even in inlets where currents are particularly strong (Olabarrieta et al., 2014). As such, the change in the location of breaking is expected to be most strongly connected to the change in the location of the underlying bathymetric feature that instigates depth-limited breaking.

Studies of tidal inlets, deltas and other energetic coastal environments have particularly benefited from remote sensing. X-band systems are increasingly deployed in concert with other remote sensing technologies and in-situ instrumentation to examine the otherwise undersurveyed evolution of coastal features of varying scales (Ruessink et al., 2002; Holman and Haller, 2013; Montreuil et al., 2014; Hessner et al., 2014)

The high spatial and temporal resolution of remotely collected data in these environments has allowed forcing mechanisms to be connected directly to morphologic evolution (Balouin et al., 2001; Díaz et al., 2014; Pianca et al., 2014).

### 1.2. Geographic setting

Oregon Inlet (35.779°N, −75.532°W) is a large inlet system located on the Outer Banks of Dare County, North Carolina. The inlet divides Bodie Island (currently a large spit) to the north from Pea Island (currently connected to Hatteras Island) to the south (Fig. 1). Following its formation during a storm in 1846, Oregon Inlet rapidly and consistently migrated south at a rate of up to two kilometers per 100 years (Miller et al., 1997). In 1991, the U.S. Army Corps of Engineers Wilmington District (USACE-SAW) built a ~1 km terminal groin along the northern end of Pea Island to protect the bridge ramp from further inlet migration (Overton et al., 1993).

The wave climatology at Oregon Inlet consists of periodic high-wave (> 3 m) events - tropical and extratropical storms - that have historically forced a net southward transport in this coastal area, although this trend can vary seasonally (Inman and Dolan, 1989). While the actual

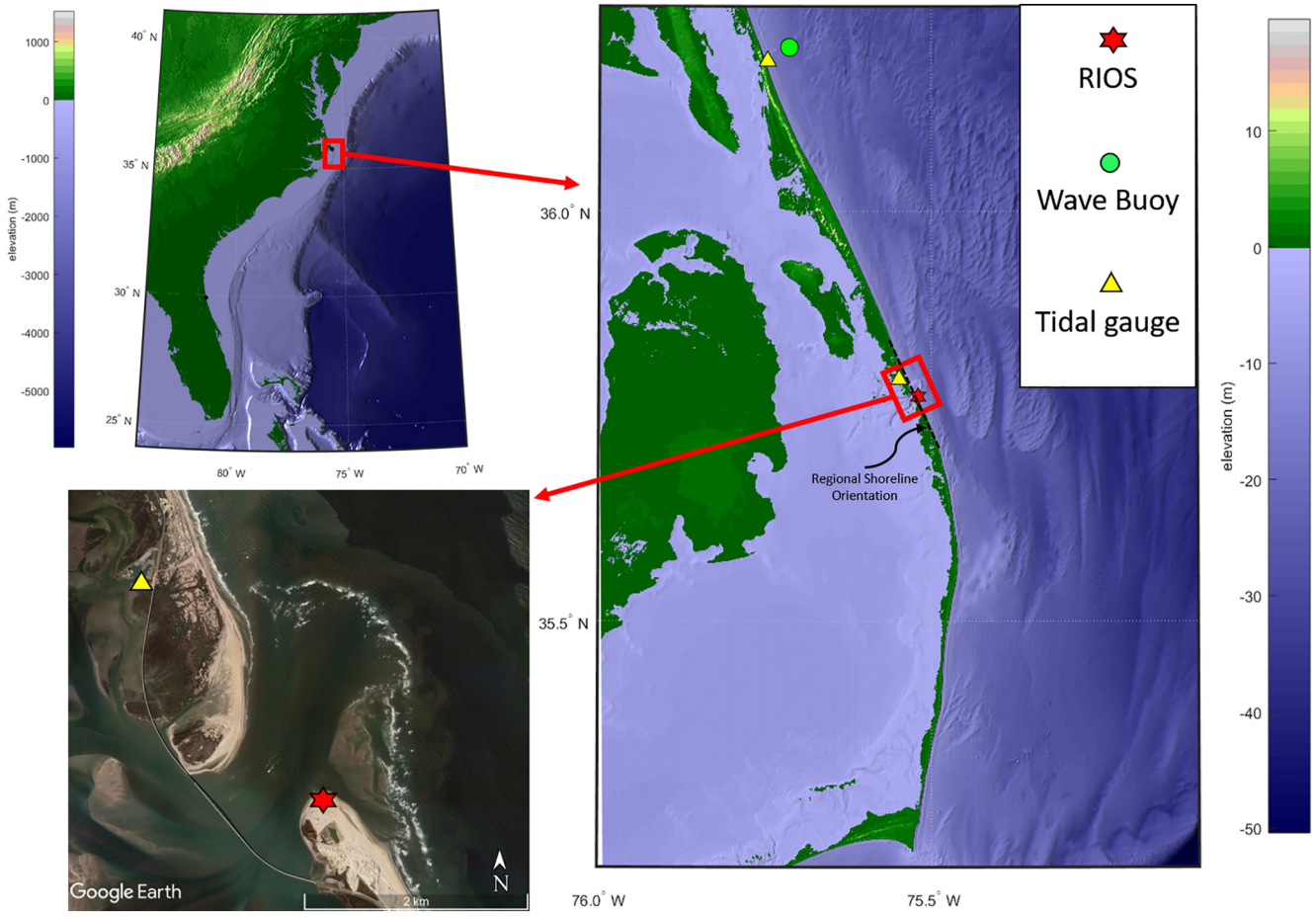


**Fig. 1.** (Top-left panel) The Outer Banks are located near the middle of the U.S. East Coast and protrude to near the edge of the continental shelf. (Right panel) Oregon Inlet is located along the northern Outer Banks between Bodie Island (to the North) and Pea Island (to the South). The regional shoreline orientation is marked by a dashed black line. Water level and wave property records were obtained from instruments located near the FRF approximately 48 km north of Oregon Inlet. (Bottom-left panel) In this Satellite imagery of Oregon Inlet, the bridge spanning the inlet may be seen, as well as wave breaking around the entire perimeter of the ebb-tidal delta. The position of a RIOS during this study and the Oregon Inlet Marina tidal gauge are marked.

volume of sediment transported along the coast is not well constrained, rough estimates based on wave energy suggest a net southward flux of 282,285 $m^3$ per year (Dolan and Glassen, 1973). The USACE-SAW conducts a monthly survey of the navigational channel and attempts to maintain a 14 ft. (4.25 m) draft clearance by nearly continuous dredging. However, the natural inlet channel has migrated to the south away from the intended navigation route such that it is pinned nearly against the terminal groin (McNinch and Humberston, 2019).

The mean tidal range is approximately 0.98 m on the ocean side of Oregon Inlet (measured at the USACE Field Research Facility in Duck, NC, about 48 km to the north), and 0.28 m on the bay side (measured at the Oregon Inlet Marina located on the back side of Bodie Island 2.5 km north of the inlet). The inlet connects the Atlantic Ocean to the large Pamlico and Albemarle Sounds to the west of the Outer Banks, and is the only hydraulic connection between the two water bodies for nearly 200 km. The coastline around Oregon Inlet is subjected to a markedly strong and highly variable wave climate for the U.S. East Coast. Consequently, Oregon Inlet's ebb delta is considered wave dominated with a small volume relative to its expansive flood delta. Although the installation of the groin has stopped the erosion on Pea Island, the Oregon Inlet channels and delta systems continue to be dynamic. The main channel and surrounding bedforms continually meander and dramatic inlet rearrangements frequently occur during large storm events (Dolan and Glassen, 1973).

### 1.3. Wave induced longshore sediment transport

Komar and Inman (1970) and Komar (1971) used concepts of wave radiation stress (Longuet-Higgins and Stewart, 1964; Longuet-Higgins, 1970) to derive a simple equation directly estimating volumetric longshore sediment transport from breaking wave parameters.

$$Q_s = K_1 H_b^{5/2} \cos(\phi_b - \theta) \sin(\phi_b - \theta) \quad (1)$$

where $Q_s$ is the volumetric sediment transport rate (in $m^3$ per time interval, often reported as $m^3$/day), $H_b$ is the height (in m) of waves at their breaking point, $\phi_b$ is the breaking wave crest angle (relative to true N), $\theta$ is the shoreline orientation (also relative to true N), and $K_1$ is an empirical constant relating the driving forces to the sediment flux approximated by 0.4 $m^{1/2}$/s for quartz sand (Komar, 1998; Rosati et al., 2002).

Recognizing that $H_b$ is not necessarily uniform along the coast (particularly where there are dynamic coastline shapes present), Ashton and Murray (2006) further modified Eq. (1) to estimate sediment transport from offshore wave properties.

$$Q_s = K_2 H_o^{12/5} T^{1/5} \cos^{6/5}(\phi_o - \theta) \sin(\phi_o - \theta) \quad (2)$$

where $K_2$ is a function of $K_1$ and the ratio of wave height to water depth (assumed to be 0.42 after Komar and Inman, 1970, and consistent with Sallenger and Holman, 1985) for breaking waves (Komar, 1998), $H_o$ is the wave height in deep water, $T$ is wave period, and $\phi_o$ is deep water wave angle. The derivation assumes that refraction occurs over shore

parallel depth contours, breaking waves are fully shallow water waves, and wave breaking is depth limited. These approximations are assumed reasonable along gently sloping passive margins like the U.S. eastern coastline offshore the Outer Banks and are used herein to estimate sediment transport rates in the vicinity of Oregon Inlet using wave properties measured at an offshore buoy.

## 2. Methods

### 2.1. X-band measurements

Observations of ebb-tidal delta morphology and bedform migration were obtained with a Radar Inlet Observation System (RIOS), a mobile X-band radar system (McNinch et al., 2012; McNinch and Humberston, 2019) deployed on the terminal groin of the southern side of Oregon Inlet from 21 July 2016 through 16 May 2017. The radar footprint covered a 6 km diameter semi-circle encompassing the inlet and ebb-delta systems. Raw backscatter was collected for 10 min each hour at a sampling rate of approximately 0.83 Hz (with very minor variations due to wind). In total, 512 radar antenna rotations were completed during each sampling period and consisted of 514 azimuthal beams, each composed of 1024 evenly spaced range samples over the 3 km radius. The polar coordinate referenced data were gridded to a 5 m Cartesian grid with the x and y axes oriented to the best estimate of the cross-shore (shore-normal) and longshore (shore-parallel) directions, respectively. The regional orientation of the shoreline was estimated to be 152° CW relative to true north based on the regional shoreline orientation of the Outer Banks near Oregon Inlet (Fig. 1, top right panel).

Gridded intensity values were averaged over each hourly 10-min collection to produce an hourly time-averaged backscatter product primarily representing wave shoaling and breaking patterns. A 25 h running average filter was applied to these hourly time-averaged images to smooth the periodic horizontal migration of wave breaking patterns due to dominant M2 tidal constituent (Holman and Stanley, 2007). Resulting 25 h filtered images produced a more robust representation of wave shoaling patterns and thus a more realistic approximation of the underlying morphology. Finally, a flat structuring element (binary valued neighborhood) was created using a disk method surrounding each pixel of the averaged returns to approximate lingering mechanically spawned background trends which were then removed to accentuate water surface related features (Fig. 2; Van Den Boomgaard and Van Balen, 1992).

While wave breaking locations are expected to be primarily dictated by the underlying morphology, other processes such as wave-current interactions may also shift the breaking location (Olabarrieta et al., 2014). Therefore, without further verification, areas with high levels of continuous backscatter associated with wave breaking are considered implied bedform locations (henceforth shortened to IBL) as there is yet some ambiguity in the exact relation between the backscatter maximum and morphological features.

### 2.2. Morphodynamic analysis

The areas over land and within the sound were voided in the temporally smoothed 25-hour intensity images. The remaining field of view was then analyzed from Eulerian and Lagrangian perspectives to estimate the migratory rates and directions of IBL. In the first (Eulerian) method an optical flow tracking algorithm was applied to the daily averaged images to estimate the flow (following Farnebäck, 2003). Various forward stepping intervals ranging 2 to 25 h were used in the optical flow algorithm, with a 4 h interval chosen to allow appreciable morphologic evolution without overly smoothing fine scale changes. The migration patterns of the IBL resulting from this analysis were decomposed into their cross-shore and longshore components relative to the estimated regional shoreline orientation.

The *sec*ond method followed specific bedforms using a Lagrangian approach in the form of longshore and cross-shore oriented Hovmoller diagrams, also known as timestacks (Shand et al., 1999). Timestacks with spatial extent of 1200 m were created along the x and y axes over a staggered grid designed to minimize overlap (Fig. 3). Coherent increased intensity returns due to consistent wave shoaling and breaking signified the presence of a bedform. These features could be tracked through space (in orthogonal directions) and time. In each timestack that contained at least one clear bedform migratory path, the most complete path within the timestack's spatial extent was coarsely manually marked (Fig. 4-magenta). In each case, the cross-shore and alongshore movements were chosen independently and so do not necessarily reflect the same bedform but only an orthogonal component within the same area. The periodically chosen positions were interpolated onto each timestep to create a continuous digitized bedform path (Fig. 4-black). A local maxima filter was applied to the continuous manually selected paths to capture the finer scaled variations of bedform movements (Fig. 4-green). In cases where no bedform path could be clearly identified or distinguished from other bedform paths, none were extracted.

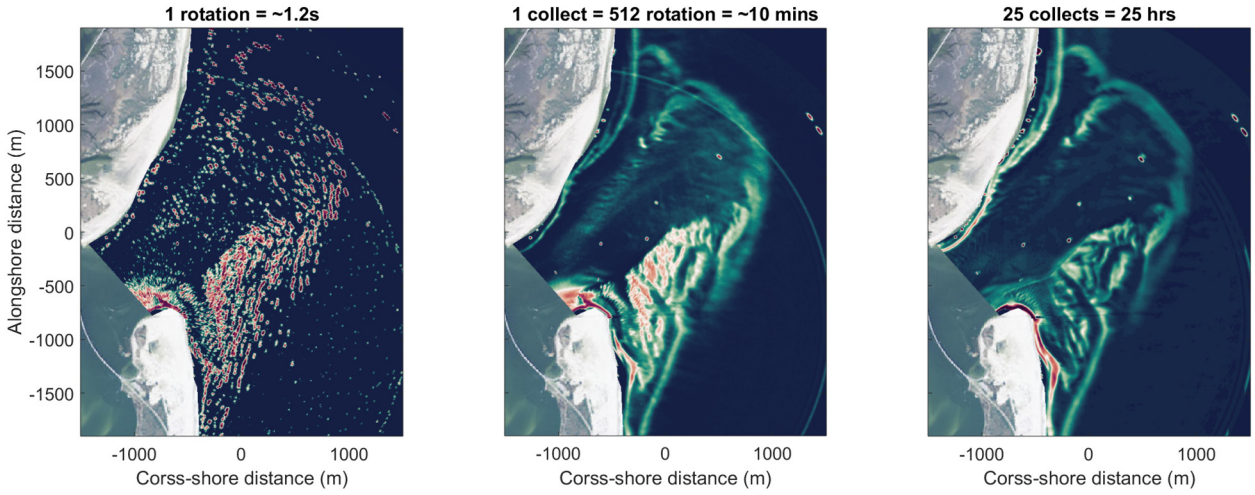


**Fig. 2.** (Left panel) Example of the relative X-band backscatter from a single antenna rotation (which takes place over approximately 1.2 s) at Oregon Inlet. Ligher colors signify higher return intensity and darker colors lower or no return intensity. The intensity of the return signal represents the near instantaneous wave shoaling and breaking patterns. (Middle panel) The average backscatter intensity from a 10-minute (512 rotation) collection. (Right panel) Example 25 h filtered product of the 10-minute average intensities used to smooth the lateral shifts in wave breaking due to changes in water depth of tidal cycles.

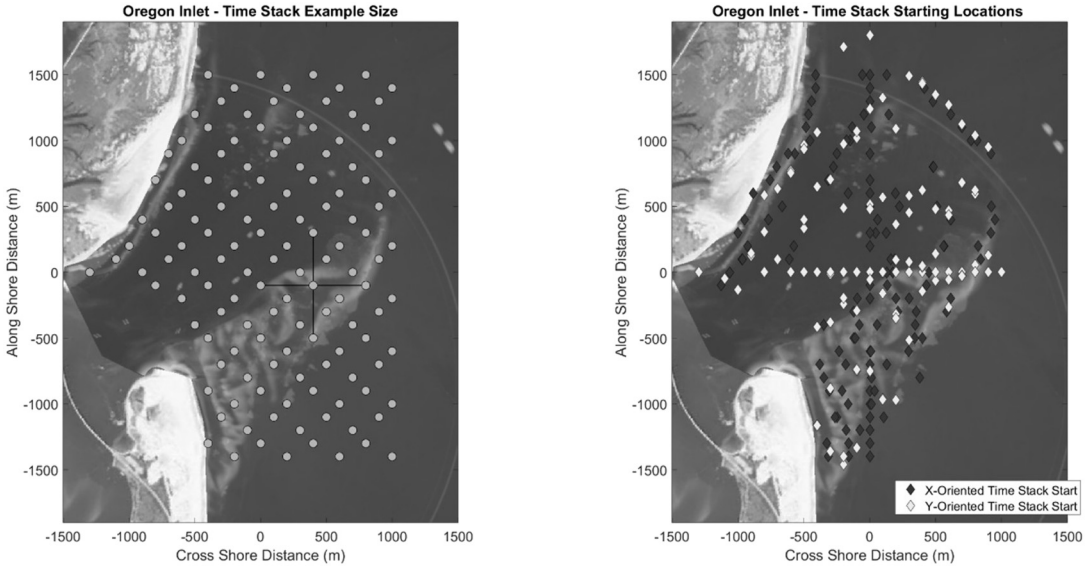


**Fig. 3.** (Left panel) Predetermined locations where timestacks were created. The black lines show an example of the cross-shore and longshore orientation and reach of the timestacks. Timestacks overlap 50% with the next timestack in each direction so that bedform paths extending off the edge of one may be marked in their entirety in the adjacent timestack. (Right panel) Starting locations of bedforms migratory paths picked within timestacks. X (cross-shore) and Y (alongshore) oriented timestacks were differentiated as they did not necessarily depict the same bedform.

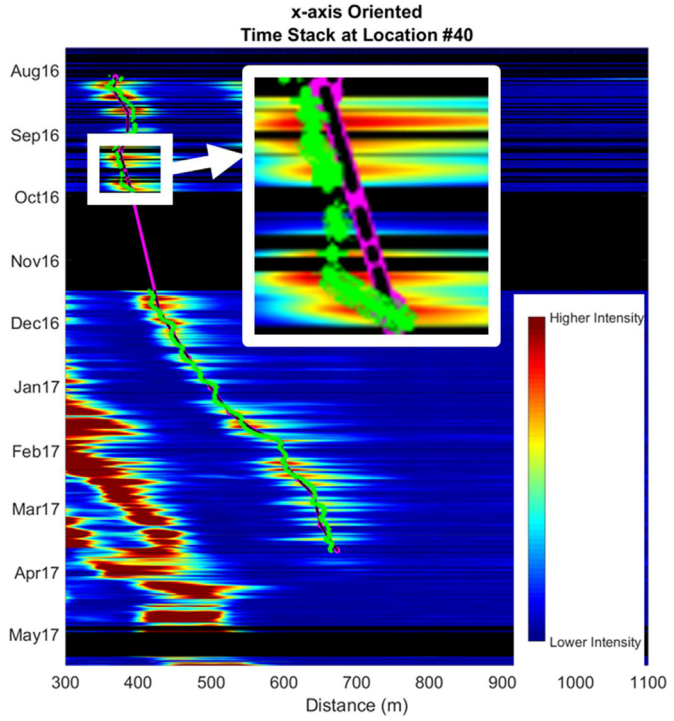


**Fig. 4.** An example of a cross-shore oriented timestack. The colormap represents the averaged backscatter intensity in which peaks represent the location of a bedform. The zoomed in subset shows an example area of the manually picked bedform path through time (magenta), the path interpolated only during period the radar was active (black) and the path picked by applying a local maxima filter (green). (For interpretation of the references to colour in this figure legend, the reader is referred to the web version of this article.)

### 2.3. Longshore sediment transport

Time series of wave statistics were obtained from a Datawell Directional Waverider buoy (NDBC station #44100) located in 26 m water depth seaward of the coast of the USACE FRF in Duck, 48 km north of Oregon Inlet. Wave statistics from the buoy include significant wave height (in m), peak and mean wave period (in sec) and peak and mean wave direction (in degrees from true N). The Oregon Inlet Buoy (NDBC station #44095) located nearly directly offshore from Oregon Inlet was offline for substantial portions of the study period; however, time periods when data were available from both buoys were compared to determine mean differences in wave statistics and an assessment of the usefulness in using the more distant Duck wave buoy data. The average difference between the FRF and Oregon Inlet wave direction measurements was 5.8°. This was added to the wave angle recorded at the FRF buoy to account for the bulk lateral variation in wave angles from the buoy location to offshore of Oregon Inlet. An analysis of the effects of the spatial separation between the buoy used to make wave measurements and the inlet's location was conducted and results are discussed in Appendix A.

The wave records were used to estimate longshore volumetric sediment transport in the nearshore region using Eq. (2) with the deep-water wave height approximated by the observed significant wave height, the deep-water wave period assumed to be the average wave period and the deep water wave angle assumed to be the average wave angle.

## 3. Results

### 3.1. Bedform migratory patterns

Migration rates and directions estimated from the Eulerian optical flow tracking algorithm were averaged from 16 November 2016 to 01 April 2017, a period with no data lapses, to examine long-term migration patterns (Fig. 5). The analysis revealed complex but spatially coherent migration patterns which suggest the various IBL are migrating in recurring patterns over time.

There is a migration of the IBL towards the inlet within the northern marginal flood channel (along the coast of Bodie Island). This is consistent with the dominant direction of alongshore sediment transport due to wave activity as well as the tidally controlled direction of flow expected in this channel. Sand bar like features were observed along this section of coast and became increasingly perpendicular to the coast and the inlet's throat towards the terminus of Bodie Island. The inlet directed migration of bedforms along the northern coast is interrupted by an area of reverse bedform migration (Fig. 5, location A). This area

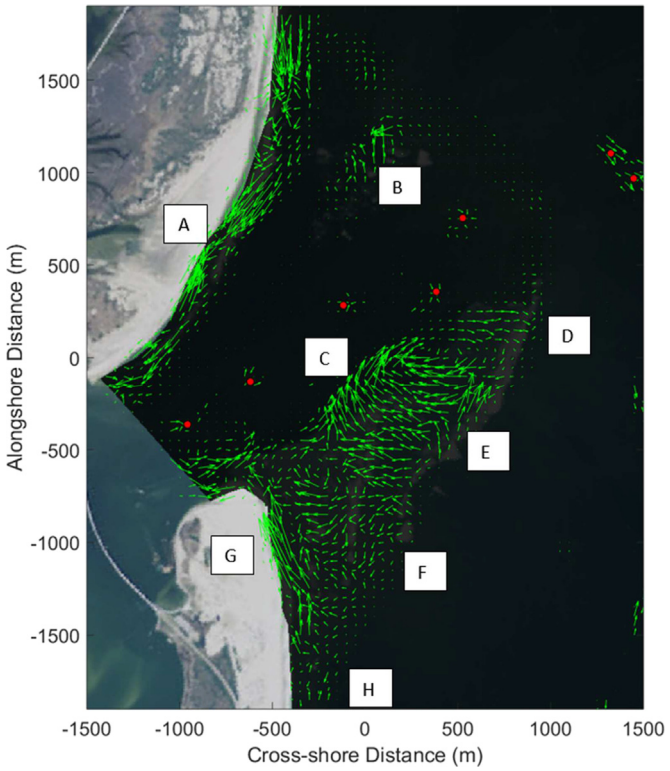


**Fig. 5.** Temporally averaged direction and relative magnitude of bedform movements (green arrows) for a period from 16 November 2016 to 01 April 2017. Migration patterns and rates were obtained using an optical motion tracking algorithm on successive 25-hour averaged intensity images. The red dots mark the location of the channel marker buoys which introduce artificial migration indicators in their immediate vicinity. Letters mark areas of interest (see text for explanation). (For interpretation of the references to colour in this figure legend, the reader is referred to the web version of this article.)

coincides with the mouth of a minor second channel that periodically opens, generally during storm events.

A long (> 1000 m), narrow (~250 m) and relatively linear shoal feature (channel margin linear bar) existed seaward of Bodie Island's coast and separated the marginal flood channel from the main ebb channel (Fig. 5-B). This feature was observed through much of the study period and averaged radar images suggest it was superimposed with sand waves with roughly 60 m wavelengths. However, due to significant wave dissipation over the terminal lobe, wave shoaling and breaking patterns were only consistently recorded on the seaward end of this linear shoal feature and so the motions of IBL along the landward segment of the bar are not well captured in the averaged flow analysis results. The IBL movements over this inner part are periodically captured and during such times were consistently migrating seaward. The migratory patterns on the seaward edge of this shoal, which were captured by the optical flow analysis, show a recirculation pattern where bedforms migrating seaward curve northward and then landward, presumably as the channel focused ebb current dissipates into the surrounding waters (Fig. 5-B).

To the south of the main ebb channel is a large shoal complex. It is markedly larger than the solitary channel margin linear bar to the north of the channel. The optical flow analysis shows that the movement of the breaking patterns on the southern shoal complex is also more dynamic than those on the northern shoal. Along the southern edge of the main ebb channel, IBL were continuously migrating seaward (Fig. 5-C). Like on the northern shoal, but mirrored, IBL migrating seaward begin to curve away from the main ebb channel near the terminal lobe, again likely due to a dispersing ebb-current (Fig. 5-D). The large portion of the center of the southern shoal complex (Fig. 5-E) shows evidence of IBL migrating back towards the main ebb channel. In combination with the seaward portion of the complex, this forms a circular and rotating migration pattern of the IBL. Further landward on the shoal complex (Fig. 5-F) the IBL migration directions begin to orient towards the shoreline. Along the coast of the southern island (Pea Island; Fig. 5-G) there is a strong migratory pattern towards the inlet within the southern marginal flood channel. Further south, there is a relatively subtle migration pattern that suggests bedforms are welding to the coast of Pea island approximately 1100 m south of the inlet's southern extent (Fig. 5-H).

### 3.2. Alongshore forces acting on an ebb-tidal delta

The modeled longshore transport time series were compared with the spatially averaged alongshore migration rates of IBL estimated by the Eulerian motion tracking algorithm (Fig. 6), and found to be significantly correlated (Fig. 7; $\rho = 0.65$ with 95% confidence interval of

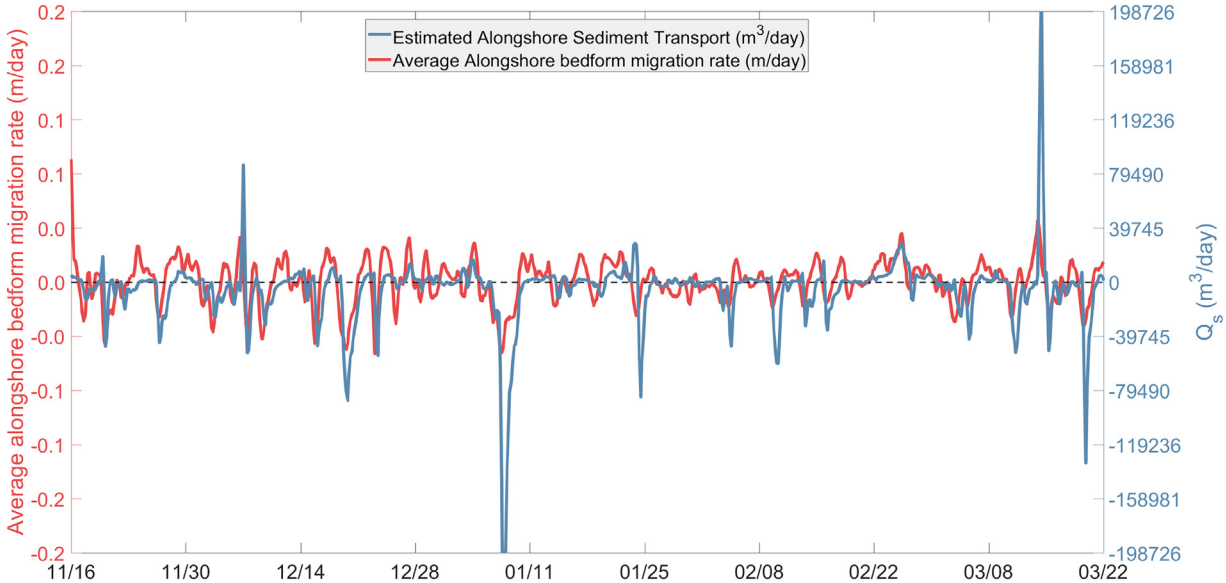


**Fig. 6.** Spatially averaged alongshore bedform migration rate (*red*; left axis), and estimated wave driven alongshore sediment transport from the Ashton and Murray (2006) derivation (*blue*; right axis). (For interpretation of the references to colour in this figure legend, the reader is referred to the web version of this article.)

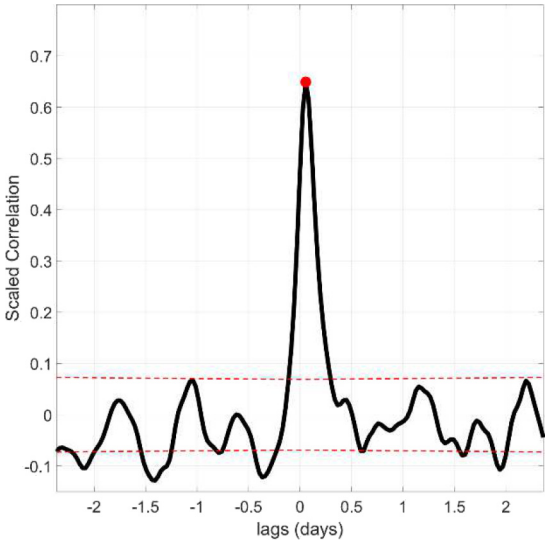


**Fig. 7.** Time lagged cross-correlation between the spatially averaged alongshore bedform migration time series and the estimated wave driven alongshore sediment transport. Maximum correlation is 0.65. 95% confidence intervals are shown with the dashed gray lines (computed using the long-lag artificial skill method of Davis, 1976).

0.08 given by the long-lag artificial skill method of Davis, 1976). This provides statistically significant evidence (explaining 45% of the variance) that the average estimated alongshore sediment transport varies concurrently with the movement of IBL on the ebb-tidal delta. The remainder of the variance not explained by the alongshore model is due to limitations to the gross sediment transport model, inaccuracies in observed IBL rates, and sediment transport unrelated to shoal migration. Additionally, the alongshore bedform movements and sediment transport may be complicated by cross-shore circulation within the inlet itself, not unreasonable considering the more complex recirculating sediment transport pathways at Oregon Inlet hypothesized by McNinch and Humberston (2019).

Individual bedform migration captured by the Lagrangian analysis of the full study period showed high variability. The average migration distance of all bedforms tracked through the analysis was 40.5 m to the south indicating a net southward transport (Fig. 8) under the assumption that transport is in the direction of shoal migration (e.g., Robinson, 1975; O'Connor et al., 2011; Pianca et al., 2014; Ridderinkhof et al., 2016). Because the timestack measurements capture the cumulative migration of bedforms, their average deviation from their starting position was compared against the cumulative estimated sediment transport rather than the instantaneous rates (Fig. 9). While many of the high frequency variations experienced on average by the system are not captured by the time-stack analysis, the bulk north to south migration rates and longer scale patterns show similar trends.

## 4. Discussion

### 4.1. Wave forcing

A significant correlation was found between the alongshore bedform movement and estimates of alongshore sediment transport based on offshore wave properties (Fig. 7). This result was based on averaging the longshore IBL migration rates over the ebb-tidal delta, greatly simplifying the complex sediment transport processes of ebb-delta shoals. The average trends depicted are certainly the culmination of more complex and localized processes. Olabarrieta et al. (2014) showed that currents over the ebb-delta are complex, consistent with the spatially resolved RIOS observations of bedform migration. Additionally, ebb tidal currents are not exclusively oriented seaward but fan out over the ebb-tidal delta. Oregon Inlet's main channel is also tilted relative to the shore-normal axis used to define the alongshore and cross-shore directions of bedform migration. Despite these complicating factors, the strong correlation between bedform movement and wave driven transport suggests that alongshore oriented wave forces strongly influences sediment transport and bedform movement on the ebb-tidal delta.

The relation between wave driven longshore transport and bedform movements at Oregon Inlet is not unexpected. Classic theory suggests swash bars (bedforms) bypass an inlet by following a continuous path along the terminal lobe of a wave dominated ebb-tidal delta due to wave action and ebb-tidal currents (FitzGerald, 1982). However, the results of the Eulerian tracking analysis of IBL suggest that there is a more complex sediment bypassing pathway controlled by a combination of wave-driven alongshore forces (as quantified by Ashton and Murray, 2006) and cross-shore forces which may consist of sub-tidal pressure gradients across the inlet, tides and wave-driven flows, as suggested in McNinch and Humberston (2019).

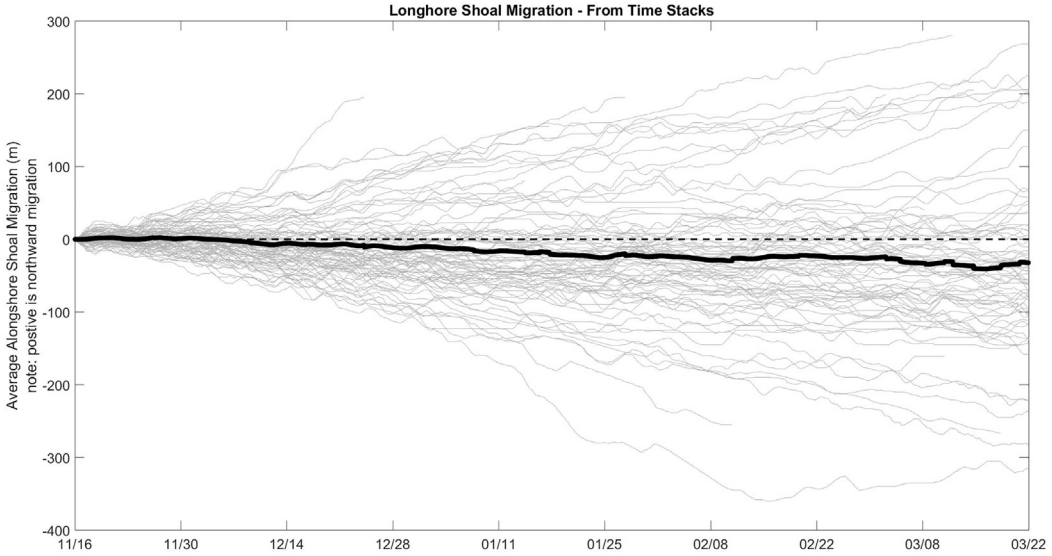


**Fig. 8.** Alongshore bedform migration distances of all the bedforms depicted in the timestacks (gray lines), and the average alongshore location of all bedforms over time (bold black line).

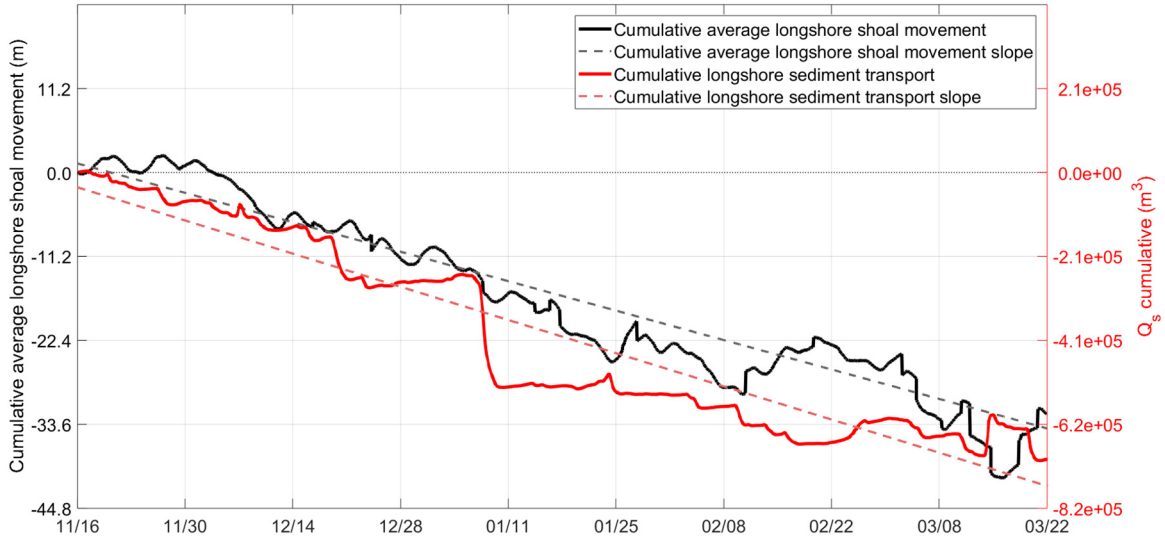


**Fig. 9.** Time series of the cumulative average longshore bedform movement magnitude (solid black line; left axis) and its linear trend (dashed black line), and the cumulative estimated alongshore sediment transport (solid red line; right axis) and its linear trend (dashed red line). (For interpretation of the references to colour in this figure legend, the reader is referred to the web version of this article.)

### 4.2. Longshore transport

Wave driven longshore transport rates were calculated using wave observations continuously obtained for 1 year between 20 Oct 2016 and 20 Oct 2017 from Ashton and Murray's Eq. (2) (Fig. 10). The average transport rate was 242 $m^3$/day with a net year-long longshore transport of 90,000 $m^3$ directed southward. This estimate is roughly consistent (within an order of magnitude) of the annual 282,285 $m^3$/yr southward transport calculated by Dolan and Glassen (1973). However, there are marked seasonal variations in wave conditions at Oregon Inlet. A 164 day time period from 20 Oct 2016 to 31 Mar 2017 spanning the fall and winter months (when RIOS observations were present and strongly correlated to Ashton and Murray's formulation) was dominated by waves from the north, resulting in net longshore transport of 904,000 $m^3$ directed southward (5512 $m^3$/day). During the ensuing 203 days from 1 Apr 2017 to 20 Oct 2017 (when RIOS observations were not present), the net transport was 814,000 $m^3$ directed northward (4099 $m^3$/day), nearly balancing the yearly net alongshore transport.

The seasonal transport rates, largely determined by the occurrence of storm events, are up to an order of magnitude larger than the yearly average. Long term averages homogenize the intermittent but dominating effects of storms, most commonly occurring from wave events out of the north (nor'easters) in the late fall and winter and out of the south (tropical cyclones) during late summer and early fall (Fig. 10). Changes in the number or intensity of storms during a season may thus substantially modify the net transport over annual time scales. The relatively small net volume of longshore transport estimated over the whole year (90,000 $m^3$) might have been coincidentally directed southward simply owing to the timing and occurrence of the storms during the analyzed time period.

The estimate of a net southward wave-driven alongshore sediment transport along this section of coast is consistent with previous studies (Dolan and Glassen, 1973; Birkemeier et al., 1985; Inman and Dolan,

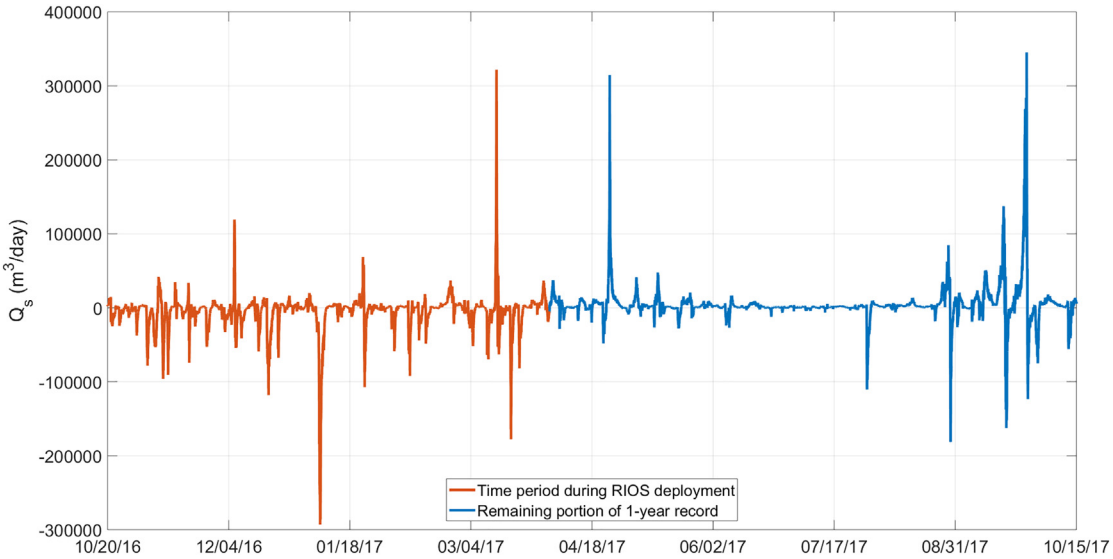


**Fig. 10.** Estimated wave driven alongshore sediment transport rate from the Ashton and Murray (2006) formulation (Eq. (2)) during a year long period from 20 October 2016 to 20 October 2017. The orange line shows the period during which RIOS was deployed and the blue shows the remaining portion of that year. Transport directions are predominantly N-to-S during the late fall, winter and early spring months and S-to-N during the later summer and early fall months. (For interpretation of the references to colour in this figure legend, the reader is referred to the web version of this article.)

1989) and further supported by the long term southern progression of Oregon Inlet until the installation of the terminal groin. The significant correlation between the alongshore sediment transport estimate and the spatially averaged migration rate of IBLs suggests that the noted wave properties driving alongshore sediment transport on open beaches are similarly influencing coherent bedform movements on Oregon Inlet's ebb delta.

Storm events can dominate both the sediment transport and bedform migration signals and at times drove estimated transport rates exceeding 200,000 $m^3$/day (using the formula of Ashton and Murray, 2006). It remains unclear whether such rates are realistic as there is no effective method to measure the representative large scale sediment transport along a section of coast. Nevertheless, it is worth considering that the simple Ashton and Murray (2006) alongshore sediment transport model captures relative trends in transport both up and down coast driven by changes in wave direction and magnitude (largely dictated by the wave height term $H_o^{12/5}$), but lacks the complexity to accurately quantify details of the sediment flux. Sophisticated numerical models are required to resolve the nature of the three-dimensional sediment transport, yet the details of sediment transport formulations used in such models are also highly dependent on parameterizations not easily validated on large time and space scales similar to those in this study. Field verification efforts are thus generally limited to comparison with observed hydrodynamics and measured (in situ) changes in bathymetry, and are the subject of ongoing research efforts.

A potential limitation to the method of remotely determining bedform location (and the subsequent implied direction of sediment transport) with RIOS is the effect of currents on wave properties. Although not expected to influence wave breaking patterns as strongly as bathymetric changes, wave-current interactions can also alter breaking locations. Currents can increase surface roughness and interact with wave orbital velocities such that patterns of waves shoaling and breaking are modified independently of morphologic change, but such shifts are expected to be minor in the alongshore direction (Haller et al., 2014). Thus, for this study, it is assumed that depth-limited wave breaking is the primary control on breaking locations (Olabarrieta et al., 2014).

## 5. Conclusions

Multi-month X-band radar measurements of breaking and non-breaking surface waves obtained with RIOS (McNinch et al., 2012) at Oregon Inlet, NC, provides an implied measure of the morphologic evolution of bedform features superimposed on the ebb-tidal delta. Using the simple alongshore sediment transport model of Ashton and Murray (2006), a time series of alongshore transport was estimated from wave parameters measured at an offshore buoy. The alongshore transport time series was compared to a spatially averaged time series of alongshore movements of implied bedform locations measured by RIOS (under the assumption that sediment transport is in the direction of shoal migration). The two records were significantly correlated ($\rho = 0.65$) suggesting that offshore wave properties are strongly influencing the alongshore migration of bedforms on the ebb-tidal delta, accounting for about 45% of the variance.

The Ashton and Murray transport formula was applied to continuous offshore wave data for a year-long period from 20 Oct 2016 to 20 Oct 2017 and estimated that a net volume of 90,000 $m^3$ was transported from north to south across the inlet. This estimate is smaller but of similar magnitude and the same direction as the 282,285 $m^3$/year estimated by Dolan and Glassen (1973). During the 164 day period when RIOS was deployed (20 Oct 2016 to 31 Mar 2017), the net alongshore transport was 904,000 $m^3$ directed southward, and during the following 201 days between 1 Apr 2017 and 20 Oct 2017 the transport was 814,000 $m^3$ directed northward, nearly balancing the yearly transport. These pronounced seasonal signals in longshore transport arising from the number and intensity of random storm events can result in high inter-annual variability that, given the correlation between transport rates and bedform movements on the ebb-tidal delta, are expected to strongly influence ebb-delta morphologic evolution at wave dominated inlets.

## Acknowledgements

This work was supported by the U.S. Army Corps of Engineers and the expert field and technical crew of the Field Research Facility in Duck, NC. J.H. was supported under the Department of Defense's Science, Mathematics & Research for Transformation (SMART) Scholarship program. Comments from the anonymous reviewers greatly improved the paper.

## Appendix A

The spatial separation between the location of the wave buoy (offshore of the FRF in 26 m depth) and Oregon Inlet was examined to assess its potential influence on transport rates. In intermediate and shallow water, waves refract due to interaction with the bottom and their angle of incidence changes. Differences in multi-year wave angle records from the Oregon Inlet (NDBC station #44095) and FRF (NDBC station #44100) buoys, separated by approximately 60 km, demonstrate that refraction patterns consistently altered the wave angles between the buoys due to their geographic separation. Wave angles measured at the buoy offshore of Oregon Inlet were an average 5.8° larger (relative to north) than those measured offshore of the FRF over a two-year period based on times when both buoys were operational. Waves of different wavenumbers and orbital velocities would experience varying degrees of refraction, but the analysis used only the average difference to account for the bulk differences in wave angles between these locations.

A simple sensitivity analysis of the effects of the bulk angle correction was conducted by computing longshore sediment transport using the FRF measured average wave angles modified by $-40°$ to 40° in 2° increments. Maximum correlations between the estimated longshore transport and average longshore bedform migration rates varied from 0.25 to 0.68 with the highest correlation occurring when angles were altered 16°. Applying a bulk rotation of 5.8° increased the correlation by 0.009 suggesting the results were not strongly influenced by using the FRF wave buoy located to the North of the inlet.

## References

Ashton, A.D., Murray, A.B., 2006. High-angle wave instability and emergent shoreline shapes: 1. Modeling of sand waves, flying spits, and capes. J. Geophys. Res. Earth Surf. 111, 1–19.

Aubrey, D.G., Giese, G.S., 1993. Formation and evolution of multiple tidal inlets. Coast. Estuar. Stud.(44) (Amer Geophysical Union. 237 pp).

Balouin, Y., Howa, H., Michel, D., 2001. Swash platform morphology in the ebb-tidal delta of the Barra Nova inlet, South Portugal. J. Coast. Res. 784, 784–791.

Barrick, D., 1972. Remote sensing of sea state by radar. Remote sensing of the Troposphere 12, 1–46.

Bass, F., Fuks, I., Kalmykov, A., Ostrovsky, I., Rosenberg, A., 1968. Very high frequency radiowave scattering by a disturbed sea surface Part II: Scattering from an actual sea surface. IEEE Trans. Antennas Propag. 16, 560–568.

Bell, P.S., 1999. Shallow water bathymetry derived from an analysis of X-band marine radar images of waves. Coast. Eng. 37, 513–527.

Bell, P.S., 2002. Determination of bathymetry using marine radar images of waves. In: Proceedings of the 4th International Symposium on: Ocean Wave Measurement and Analysis. 1. pp. 251–257 San Francisco, CA.

Bergsma, E.W.J., Conley, D.C., Davidson, M.A., O'Hare, T.J., 2016. Video-based nearshore bathymetry estimation in macro-tidal environments. Mar. Geol. 374, 31–41.

Birkemeier, W.A., Miller, H.C., Wilhelm, S.D., DeWall, A.E., Gorbics, C.S., 1985. A User's Guide to the Coastal Engineering Research Center's (CERC's) Field Research Facility. Instruction Report CERC-85-1. U.S. Army Corps of Engineers, Waterways Experiment Station, Vicksburg, MS (121 pp).

Boothroyd, J.C., 1985. Tidal inlets and tidal deltas, in: Davis Jr., R.A. (Ed.), Coastal Sedimentary Environments. Springer-Verlag, New York, pp. 445–532.

Bruun, P., 1978. Common reasons for damage or breakdown of mound breakwaters. Coast. Eng. 2, 261–273.

Catálan, P.A., Haller, M.C., 2008. Remote sensing of breaking wave phase speeds with

application to non-linear depth inversions. Coast. Eng. 55, 93–111.
Catalán, P.A., Haller, M.C., Plant, W.J., 2014. Microwave backscattering from surf zone waves. J. Geophys. Res. 119, 3098–3120.
Chen, J.-L., Hsu, T.-J., Shi, F., Raubenheimer, B., Elgar, S., 2014. Hydrodynamic and sediment transport modeling of New River Inlet (NC) under the interaction of tides and waves. J. Geophys. Res. 4028–4047.
Davidson-Arnott, R., 2010. Introduction to Coastal Processes and Geomorphology. Cambridge University Press.
Davis, R.E., 1976. Predictability of sea surface temperature and sea level pressure anomalies over the North Pacific Ocean. J. Phys. Ocean. 6 (3), 249–266.
Díaz, G.M., And, M., Haller, M.C., Raubenheimer, B., Elgar, S., Honegger, D.A., 2014. Radar remote sensing estimates of waves and wave forcing at a tidal inlet. J. Atmos. Ocean. Technol. 32, 842–854.
Dolan, R., Glassen, R., 1973. Oregon inlet, North Carolina—a history of coastal change. Southeast. Geogr. 13, 41–53.
Donelan, M.A., Pierson Jr., W.J., 1987. Radar scattering and equilibrium ranges in wind-generated waves with application to scatterometry. J. Geophys. Res. Ocean. 92, 4971–5029.
Elias, E., Stive, M., Bonekamp, H., Cleveringa, J., 2003. Tidal inlet dynamics in response to human intervention. Coast. Eng. J. 45, 629–658.
Farnebäck, G., 2003. Two-frame motion estimation based on polynomial expansion. In: Scandinavian Conference on Image Analysis. Springer, pp. 363–370.
Fiechter, J., Steffen, K.L., Mooers, C.N.K., Haus, B.K., 2006. Hydrodynamics and sediment transport in a southeast Florida tidal inlet. Estuar. Coast. Shelf Sci. 70, 297–306.
FitzGerald, D.M., 1982. Sediment bypassing at mixed energy tidal inlets. In: Coastal Engineering 1982, pp. 1094–1118.
FitzGerald, D.M., 1988. Shoreline erosional-depositional processes associated with tidal inlets. In: Hydrodynamics and Sediment Dynamics of Tidal Inlets. Springer New York, New York, NY, pp. 186–225.
FitzGerald, D.M., 1996. Geomorphic variability and morphologic and sedimentologic controls on tidal inlets. J. Coast. Res. 47–71.
FitzGerald, D.M., Kraus, N.C., Hands, E.B., 2000. Natural Mechanisms of Sediment Bypassing at Tidal Inlets. CHETN-IV-30. U.S. Army Corps of Engineers, Vicksburg, MS.
Gao, J., 2009. Bathymetric mapping by means of remote sensing: methods, accuracy and limitations. Prog. Phys. Geogr. 33, 103–116.
Haller, M.C., Lyzenga, D.R., 2003. Comparison of radar and video observations of shallow water breaking waves. IEEE Trans. Geosci. Remote Sens. 41, 832–844.
Haller, M.C., Honegger, D., Catalan, P.A., 2014. Rip Current Observations via Marine Radar. J. Waterw. Port Coast. Ocean Eng. 140, 115–124.
Hayes, M.O., 1980. General morphology and sediment patterns in tidal inlets. Sediment. Geol. 26, 139–156.
Hayes, M.O., Goldsmith, V., Hobbs, C.H., 1970. Offset coastal inlets. In: Proceedings of the 12th International Conference on Coastal Engineering. American Society of Civil Engineers, New York, pp. 1187–1200.
Herrling, G., Winter, C., 2018. Tidal inlet sediment bypassing at mixed-energy barrier islands. Coast. Eng. 140, 342–354.
Hessner, K., Reichert, K., Carlos, J., Borge, N., Stevens, C.L., Smith, M.J., 2014. High-resolution X-Band radar measurements of currents, bathymetry and sea state in highly inhomogeneous coastal areas. Ocean Dyn. 64, 989–998.
Holman, R., Plant, N., Holland, T., 2013. cBathy: A Robust Algorithm for Estimating Nearshore Bathymetry. 118. pp. 2595–2609.
Holman, R.A., Haller, M.C., 2013. Remote sensing of the nearshore. Annu. Rev. Mar. Sci. 5, 95–113.
Holman, R.A., Stanley, J., 2007. The history and technical capabilities of Argus. Coast. Eng. 54, 477–491.
Holman, R.A., Sallenger, A.H., Lippmann, T.C., Haines, J.W., 1993. The application of video image processing to the study of nearshore processes. Oceanography 6, 78–85.
Inman, D.L., Dolan, R., 1989. The outer banks of North Carolina: budget of sediment and inlet dynamics along a migrating barrier system. J. Coast. Res. 193–237.
Komar, P.D., 1971. The mechanics of sand transport on beaches. J. Geophys. Res. 76, 713–721.
Komar, P.D., 1996. Tidal-inlet processes and morphology related to the transport of sediments. J. Coast. Res. 23–45.
Komar, P.D., 1998. Beach Processes and Sedimentation, 2nd ed. 544 Prentice-Hall, Englewood Cliffs, NJ.
Komar, P.D., Inman, D.L., 1970. Longshore sand transport on beaches. J. Geophys. Res. 75, 5914–5927.
Lee, P.H.Y., Barter, J.D., Beach, K.L., Hindman, C.L., Lake, B.M., Rungaldier, H., Shelton, J.C., Williams, A.B., Yee, R., Yuen, H.C., 1995. X band microwave backscattering from ocean waves. J. Geophys. Res. Ocean. 100, 2591–2611.
Lillycrop, W.J., Parson, L.E., Irish, J.L., Brooks, M.W., 1996. Hydrographic surveying with an airborne LiDAR survey system. In: Proceedings of the 2nd International Airborne Remote Sensing Conference, pp. 279–285 San Francisco, CA.
Lippmann, T.C., Holman, R.A., 1989. Quantification of sand bar morphology: a video technique based on wave dissipation. J. Geophys. Res. Ocean. 94, 995–1011.
Lippmann, T.C., Holman, R.A., 1990. The spatial and temporal variability of sand bar morphology. J. Geophys. Res. Ocean. 95, 11575–11590.
Longuet-Higgins, M.S., 1970. Longshore currents generated by obliquely incident sea waves: 1. J. Geophys. Res. 75, 6778–6789.
Longuet-Higgins, M.S., Stewart, R., 1964. Radiation stresses in water waves; a physical discussion, with applications. Deep Sea Res 11, 529–562.
Lyzenga, D.R., 1991. Interaction of short surface and electromagnetic waves with ocean fronts. J. Geophys. Res. 96 (C6), 10,765–10,772.
Lyzenga, D.R., 1998. Effects of intermediate-scale waves on radar signatures of ocean fronts and internal waves. J. Geophys. Res. 103 (C9), 18,759–18,768.
McNinch, J., Humberston, J., 2019. Radar inlet observing system (RIOS) at Oregon Inlet, NC: sediment transport pathways at a wave-dominated tidal inlet. Shore and Beach 87 (1), 24–36.
McNinch, J.E., 2007. Bar and swash imaging radar (BASIR): a mobile X-band radar designed for mapping nearshore sand bars and swash-defined shorelines over large distances. J. Coast. Res. 59–74.
McNinch, J.E., Brodie, K.L., Slocum, R.K., 2012. Radar Inlet Observing System (RIOS): continuous remote sensing of waves, currents, and bathymetry at tidal inlets. Oceans 1–8, 14–19.
Miller, H.C., Dennis, W.A., Wutkowski, M.J., 1997. A unique look at Oregon Inlet, NC USA. In: Proceeding of the 25th International Conference on Coastal Engineering. ASCE, pp. 4517–4530.
Montreuil, A.L., Levoy, F., Bretel, P., Anthony, E.J., 2014. Morphological diversity and complex sediment recirculation on the ebb delta of a macrotidal inlet (Normandy, France): a multiple LiDAR dataset approach. Geomorphology 219, 114–125.
Munk, W.H., 1949. The solitary wave theory and its application to surf problems. Ann. N. Y. Acad. Sci. 51, 376–424.
O'Brien, M.P., Zeevaert, L., 1969. Design of a small tidal inlet. In: Proceedings of the 11th International Conference on Coastal Engineering, pp. 1242–1257.
O'Connor, M.C., Cooper, J.A.G., Jackson, D.W.T., 2011. Decadal behavior of tidal inlet-associated beach systems, Northwest Ireland, in relation to climate forcing. J. Sediment. Res. 81, 38–51.
Olabarrieta, M., Warner, J.C., Kumar, N., 2011. Wave-current interaction in Willapa Bay. J. Geophys. Res. 116, C12014.
Olabarrieta, M., Geyer, W.R., Kumar, N., 2014. The role of morphology and wave-current interaction at tidal inlets: an idealized modeling analysis. J. Geophys. Res. Ocean. 119, 8818–8837.
Overton, M.F., Fisher, J.S., Dennis, W.A., Miller, H.C., 1993. Shoreline Change at Oregon Inlet Terminal Groin. In: Proceedings of the 23rd International Conference on Coastal Engineering, pp. 2332–2343.
Pacheco, A., Vila-Concejo, A., Ferreira, Ó., Dias, J.A., 2008. Assessment of tidal inlet evolution and stability using sediment budget computations and hydraulic parameter analysis. Mar. Geol. 247, 104–127.
Pianca, C., Holman, R., Siegle, E., 2014. Mobility of meso-scale morphology on a microtidal ebb delta measured using remote sensing. Mar. Geol. 357, 334–343.
Plant, W.J., Keller, W.C., Hayes, K., Chatham, G., Lederer, N., 2010. Normalized radar cross section of the sea for backscatter: 2. Modulation by internal waves. J. Geophys. Res. 115, 9033.
Radermacher, M., Wengrove, M., van Thiel de Vries, J., Holman, R., 2014. Applicability of video-derived bathymetry estimates to nearshore current model predictions. J. Coast. Res. 70, 290–295.
Ridderinkohf, W., de Swart, H.E., van der Vegt, M., Hoekstra, P., 2016. Modeling the growth and migration of sandy shoals on ebb-tidal deltas. J. Geophys. Res. Earth Surf. 121, 1351–1371.
Robinson, A.H.W., 1975. Cyclic Changes in Shoreline Development at the Entrance to Teignmouth Harbour, Devon, England. 8. John Wiley, London, U. K., pp. 181–200.
Rosati, J.D., Walton, T.L., Bodge, K., 2002. Longshore sediment transport. In: King, D.B. (Ed.), Coast. Eng. Manual, Part II, Coastal Sediment Processes. U.S. Army Corps of Engineers, Washington, D.C. chap III-2.
Ruessink, B.G., Bell, P.S., Van Enckevort, I.M.J., Aarninkhof, S.G.J., 2002. Nearshore bar crest location quantified from time-averaged X-band radar images. Coast. Eng. 45, 19–32.
Sallenger, A.H., Holman, R.A., 1985. Wave energy saturation on a natural beach of variable slope. J. Geophys. Res. 90 (C6), 11,939–11,944.
Sallenger, A.H., Krabill, W.B., Swift, R.N., Brock, J., List, J., Hansen, M., Holman, R.A., Manizade, S., Sontag, J., Meredith, A., 2003. Evaluation of airborne topographic lidar for quantifying beach changes. J. Coast. Res. 125–133.
Shand, R.D., Bailey, D.G., Shepherd, M.J., 1999. An inter-site comparison of net offshore bar migration characteristics and environmental conditions. J. Coast. Res. 750–765.
Stockdon, H.F., Sallenger, A.H., List, J.H., Holman, R.A., 2002. Estimation of shoreline position and change using airborne topographic lidar data. J. Coast. Res. 502–513.
Thornton, E.B., Guza, R.T., 1983. Transformation of wave height distribution. J. Geophys. Res. Ocean. 88, 5925–5938.
Trizna, D.B., 1997. A model for Brewster angle damping and multipath effects on the microwave radar sea echo at low grazing angles. IEEE Trans. Geosci. Remote Sens. 35, 1232–1244.
Van Den Boomgaard, R., Van Balen, R., 1992. Methods for fast morphological image transforms using bitmapped binary images. CVGIP Graph. Model. Image Process. 54, 252–258.
Williams, W.W., 1947. The determination of gradients on enemy-held beaches. Geogr. J. 109, 76–90.
Wright, J.W., 1968. A new model for sea clutter. IEEE Trans. Antennas Propag. 16, 217–223.